Radio Science, Volume 34, Number 2, Pages 477–487, March–April 1999

Dynamics and anisotropy of traveling ionospheric disturbances as deduced from transionospheric sounding data

E. L. Afraimovich, O. N. Boitman, E. I. Zhovty,[1] A. D. Kalikhman, and T. G. Pirog

Institute of Solar-Terrestrial Physics, Siberian Division of Russian Academy of Science Irkutsk, Russia

Abstract. This paper presents the diurnal and seasonal statistics for the dynamics and anisotropy of medium-scale traveling ionospheric disturbances (MS TIDs) in comparison with the dynamics of small-scale irregularities (SSIs), using data from an annual run of ETS 2 radio signal polarization, angle-of-arrival, and scintillation measurements at 136 MHz in Irkutsk, Russia (52°N, 104°E). In daytime, phase interference patterns have the form of traveling waves with the mean propagation direction ψ equal to 160° and rms of 68°, and phase velocity of 133 ± 62 m/s. The mean value of ψ increases in a clockwise direction from southeastward to southward and opposite to the calculated direction of the neutral wind, with the spread not exceeding 10°–30°. This result is in agreement with the hypothesis of neutral wind-induced filtering of atmospheric gravity waves (AGW) and MS TIDs caused by them. It was found that at night, MS TIDs are characterized by a strong anisotropy; the direction of elongation (modulo 180°) is, on average, 25° less than for SSIs. This difference can be explained by assuming that medium-scale phase disturbances detected at night are caused by magnetic-field-aligned irregularities located in the plasmasphere.

1. Introduction

Traveling ionospheric disturbances with sizes ranging from a few hundred kilometers to a thousand kilometers are of interest for scientific inquiry into ionospheric physics and as a factor that limits the accuracy of modern-day radio engineering systems used in navigation and radio interferometry; a rich variety of publications has addressed the subject of TIDs (see review by *Hocke and Schlegel* [1996]). The central problem of TID research is to seek the main geophysical factors governing the structure and dynamics of these disturbances.

One such factor is the neutral wind. According to an earlier filtering hypothesis [*Hines and Reddy*, 1967], its action manifests itself in filtering of atmospheric gravity waves (AGWs), with TIDs being their ionospheric response, along the propagation direction. The earliest reliable experimental evidence for TID filtering along propagation directions was provided by observations from 1975 to 1976 obtained in the northern hemisphere through vertical-incidence HF soundings of the ionospheric F_2 region during the daytime using the angle-of-arrival and Doppler methods [*Kalikhman*, 1980]. Subsequently, some authors reported the detection of the filtering effect for the daytime hours in doing ground-based ionospheric radio soundings, with a rea-

[1]Deceased July 28, 1996.

Paper number 1998RS900004.
0048-6604/99/1998RS900004$11.00

sonable degree of certainty [*Waldock and Jones*, 1986; *Crowley et al.*, 1987]. Verification of the filtering hypothesis received considerable attention in publications on TIDs observed by transionospheric VHF soundings [*Mercier*, 1986, 1996; *Jacobson et al.*, 1995]. These authors have presented observations which do not support this hypothesis. So experimental research and modeling of the filtering effect have not yet reached a point where the filtering process is trustworthy and its origin adequately understood. The resolution of this issue would substantially improve the diagnostic capabilities of remote radio probing of the atmosphere.

The Earth's magnetic field is another important factor that determines the structure and dynamics of ionospheric irregularities. The magnetic field effect is most clearly manifested in the structure and dynamics of small-scale irregularities (SSIs) of a size typically between 0.1 and 1.0 kilometers. The most reliable SSI velocity and anisotropy measurements at midlatitudes were made by spaced-antenna reception of transionospheric radio signals from discrete radio sources and radio beacons on navigational-aid and geostationary satellites.

Traditionally, experimental research into the origin of two irregular features so different in size (TIDs and SSIs) has been done without any special correlation with each other. New data were obtained by *Jacobson et al.* [1996], which reported intriguing results on magnetically oriented irregularities of an intermediate size (10–100 km). The goal of this paper is to present results derived by investigating the anisotropy and dynamics of medium-scale traveling ionospheric disturbances (MS TIDs) in comparison with the dynamics of SSIs based on transionospheric sounding data as obtained in Irkutsk, Russia, in 1989–1990. Results are discussed and compared with data reported by other authors throughout all sections of this paper.

2. A General Characterization of the Experiment

The above mentioned statistical results are based on analysis of data from a transionospheric radio interferometer (TIR) at the Institute of Solar-Terrestrial Physics of the Russian Academy of Sciences [*Afraimovich et al.*, 1991]. This instrument is designed for simultaneous measurements at 136 MHz of the main parameters of radio signals from the Japanese geostationary satellite ETS 2 located at 130° ± 0.5°E (polarization, angle of arrival, frequency Doppler shift, and amplitude have 30-s time resolution, and amplitude scintillations have 0.2-s time resolution).

A detailed description of the interferometer, the method of data pretreatment, and the estimation of the sensitivity of measurements are given by *Afraimovich et al.* [1991]; at this point, however, we examine only the characteristics of importance for the presentation of material.

Three receiving points A, B, and C of the radio interferometer were located at apexes of a nearly right angle triangle, with sides about 200 m long. The receiving antennas of channels A, B, and C were spiral antennas of a single polarization, with about 30-dB gain. In addition, the central point A incorporated an additional antenna D, of opposite polarization. The set of A, D was used to measure the phase difference $\Delta\phi$ between antennas A, D, which was proportional to the value I of total electron content (TEC) along the line of sight (LOS) to the satellite (Faraday rotation measurements).

The value of I in units of 10^{16} m^{-2} at 136 MHz is determined from the phase difference $\phi_{AD} = \phi_A - \phi_D$ ("oblique TEC"):

$$I = 1.73 \times 10^{-2} \phi_{AD} \qquad (1)$$

where ϕ_{AD} is measured in degrees [*Davies*, 1980; *Afraimovich et al.*, 1991].

The set of A, B, C formed part of the system for measuring time variations of the phase difference $\Delta\phi$ along baselines CB and AB, proportional (subsequent to the filtering procedure described below) to values of the horizontal components I'_x and I'_y of TEC gradient, where x and y are directed eastward E and northward N, respectively.

The value of I'_x in units of 10^{11} m^{-3} at 136 MHz in our case is

$$I'_x = 1.61 \times \phi'_x \quad (2)$$

where ϕ'_x is measured in mrad/m [*Afraimovich et al.,* 1991]. For convenience of the presentation, we use phase derivatives with respect to space (mrad/m) as well as horizontal components of TEC gradient (cubic meters). In addition, amplitude scintillations with a time constant of 0.2 s were recorded simultaneously from the same antennas.

To determine characteristics of the dynamics and anisotropy of MS TIDs using the method described in section 3, the continuous series $\Delta\phi_{AB}(t)$, $\Delta\phi_{CB}(t)$, and $\Delta\phi_{AD}(t)$ of at least a 2-day duration were high-pass filtered out in order to eliminate diurnal trends in the measured quantities and those introduced by slow diurnal changes in the satellite position in geostationary orbit and variations in the regular ionosphere. The range 30–60 min was largely used, which lies within the generally accepted range of TID periods caused by AGWs [*Georges*, 1968].

Filtered series of $\Delta\phi_{AB}$, $\Delta\phi_{CB}$, and $\Delta\phi_{AD}$ were used to determine TIDs-induced TEC disturbances $\delta I(t)$ and variations of the phase derivatives ϕ'_x and ϕ'_y. Variations of the phase time derivative $\phi'_t(t)$ were determined from the derivate of $I(t)$. By testing the interferometer, it was found that its sensitivities when measuring disturbances of $I(t)$ and gradient components $I'_x(t)$ and $I'_y(t)$ in the range of 30–60 min periods were about 5×10^{13} m^{-2} and 10^{10} m^{-3}, respectively. In terms of spatial derivatives and the time derivative, corresponding threshold sensitivity values were not worse than 0.04 mrad/m and 1.85 mrad/s.

The measurements were made on a continuous and 24-hour basis since December 1989, when the interferometer became operational, to December 1990, when the transmission of the 136-MHz signal from ETS 2 was discontinued for technical reasons. As a result of sampling, when investigating the diurnal dependence of the TIDs parameters under investigation, only about 120 days, more or less uniformly distributed over the seasons of the year, were handled. The data for the winter period cover December 1989 and December 1990. In the statistics to be discussed below, in winter there are about 17 total days; in spring, summer, and fall there are 35, 26, and 42 days, respectively.

For comparing the dynamics of MS TIDs and SSIs, we processed all scintillation records taken through spaced-antenna reception, satisfying the criteria of data standard correlation handling (a total of 1318 6-min records). During the observing period the geomagnetic field was characterized by moderate values of the Kp index. The mean value of Kp is 2.36; the rms value is 1.18.

3. Data Processing

The correspondence of space-time phase characteristics in the antenna system's plane, obtained through transionospheric soundings, with local characteristics of disturbances in the ionosphere is considered in detail in a number of publications [*Georges and Hooke*, 1970; *Afraimovich et al.,* 1994; *Mercier*, 1996] and is not analyzed at length in this study. The most important conclusion of the cited references is the fact that, as for the extensively exploited model of a "plane phase screen", TEC disturbances $\Delta I(x, y, t)$ detected at a transionospheric sounding faithfully copy the horizontal part of the corresponding disturbance of local concentration and can be used in experiments on measuring the TID propagation velocity.

In the simplest form, space-time variations in phase $\Delta\phi(x, y, t)$ of the transionospheric radio signal that are proportional to TEC variations $\Delta I(x, y, t)$ in the ionosphere at each given time t can be represented in terms of the phase interference pattern that moves without a change in its shape (the nondispersive disturbances):

$$\Delta\phi(x, y, t) = F(t - x/v_x - y/v_y) = F(\varphi) \quad (3)$$

where v_x and v_y are the velocities of intersection of the phase front of the axes x and y. In real situations the ideal model (equation (3)) is not realized because the AGWs that cause TIDs propagate in the atmosphere in the form of dispersing wave packets with a finite width of the

angular spectrum. In the first approximation, however, on a short time interval of averaging (in our case 120 min) compared with a time period of filtered variations of TEC (30-60 min), the phase interference pattern moves without a substantial change in its shape.

Mercier [1986, 1996] suggested two approaches to determining the propagation direction α of the phase interference pattern. One involves determining a series of instantaneous values of the direction $\alpha(t)$, counted from the north in a clockwise direction

$$\alpha(t) = \arctan(\phi'_x(t)/\phi'_y(t)) \tag{4}$$

where ϕ'_x and ϕ'_y are the first phase derivatives with respect to the spatial coordinates x and y at the reception point, and constructing subsequently, on a chosen time interval, the distribution function of azimuth $P(\alpha)$. The central value of α is used by Mercier as an estimate of the azimuth of prevailing propagation of the phase interference pattern.

The other approach is based on determining the contrast of the interference pattern. In this case the ratio C_{XY} is calculated.

$$\begin{cases} C_{XY} = \sigma_X/\sigma_Y, & \text{if } \sigma_X > \sigma_Y \\ C_{XY} = \sigma_Y/\sigma_X, & \text{if } \sigma_Y > \sigma_X \end{cases} \tag{5}$$

where X and Y are series of the transformed values of $\phi'_x(t)$ and $\phi'_y(t)$, obtained by rotating the original coordinate system (x, y) by the angle β

$$\begin{cases} X(t) = \phi'_x(t)\sin\beta + \phi'_y(t)\cos\beta \\ Y(t) = -\phi'_x(t)\cos\beta + \phi'_y(t)\sin\beta \end{cases} \tag{6}$$

and σ_X and σ_Y are the rms of the corresponding series. *Mercier* [1986] showed that it is possible to find a value of the rotation angle β_0, at which the ratio C_{XY} will be a maximum and equal to the value of contrast C. This parameter characterizes the degree of anisotropy of the phase interference pattern. The angle β_0 in this case indicates the direction of elongation, and the angle $\alpha_c = \beta_0 + \pi/2$ indicates the direction of the wave vector $\vec{K}$ coincident (modulo 180°) with the propagation direction of the phase front.

A statistical, angle-of-arrival and Doppler method (SADM) is proposed by *Afraimovich* [1998] for determining characteristics of the dynamics of the phase interference pattern. SADM implies that we measure not only the spatial phase derivatives but also make use of the time derivative of the radio signal phase $\phi'_t(t)$ at the reception point. This permits us to ascertain the unambiguous orientation of $\psi(t)$ of the wave vector of phase disturbance in the range 0°–360° and determine the velocity modulus $v(t)$ of the phase–front propagation at each specific instant of time by the formulas

$$\begin{aligned} W_y(t) &= \phi'_y(t)/\phi'_t(t) = |W|\cos\psi \\ W_x(t) &= \phi'_x(t)/\phi'_t(t) = |W|\sin\psi \\ v(t) &= |W|^{-1} = \left(W_x^2(t) + W_y^2(t)\right)^{-1/2} \end{aligned} \tag{7}$$

Ideally, in the case of moving phase interference pattern (eqution (3)), the transformations (equation (7)) give a time constant value of azimuth and velocity, and distribution functions show a well-defined maximum at these values, because

$$\begin{aligned} \phi'_x(t) = -F'_\varphi/v_x; \qquad \phi'_y(t) = -F'_\varphi/v_y; \\ \phi'_t(t) = F'_t = F'_\varphi \end{aligned} \tag{8}$$

In practice, instantaneous values of v and ψ that were determined every 30 s were used in our case to construct, on a selected time interval (120 min), not only distribution functions of the azimuth $P(\psi)$ (as suggested by *Mercier*, [1986]), but also the velocity $P(v)$. Then $P(\psi)$ were analyzed to establish the prevailing direction of motion of the interference pattern. When it exists, the pattern can be considered as traveling, and the mean travel velocity can be determined from the $P(v)$ distribution or by directly averaging the $v(t)$ data set. Different existence criteria for a pronounced direction of displacement can be chosen; however, it would be most natural to estimate the rms of the azimuth. If the rms exceeds 90°, then it is beyond reason to speak of the directed motion of the interference pattern. If, however, the rms is markedly less than 90°, then it is reasonable to suggest that

the pattern is displaced mainly in the direction of the mean value of the azimuth.

The basic objective of this study is to examine the statistics of the diurnal and seasonal dependence of TID dynamics characteristics. In this connection, the data processing involved an hourly treatment of the data for all selected days of the 1-year period analyzed, followed by averaging for each of the seasons. In this case, for each hour, mean values of all parameters were averaged on a 2-hour interval (240 counts), and mean values were ascribed to the middle of this interval.

The velocity v and the direction of propagation ψ of the amplitude diffraction pattern with simultaneous spaced-antenna reception of ETS 2 signal scintillations under nighttime conditions are used in this paper to compare with similar results for MS TIDs. The algorithm for correlational treatment of scintillation data is given by *Afraimovich et al.* [1994b]. Analysis of our data showed that maximum correlation coefficients are close to 1.0. The drift velocities presented in this paper were obtained for maximum cross-correlation coefficients exceeding 0.6.

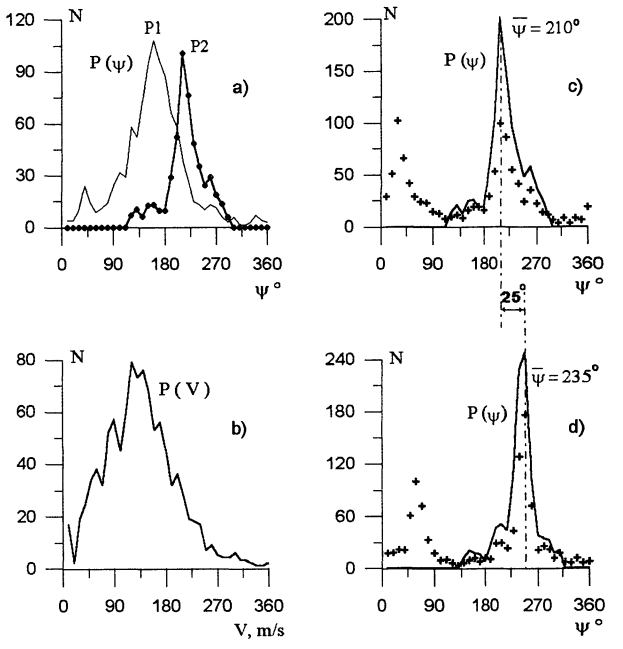

Figure 1. Shown are summary distributions. Plain solid line in Figure 1a shows azimuths $P(\psi)$ (P1), and solid line in Figure 1b shows velocities $P(v)$ of medium-scale traveling ionospheric disturbances (MS TIDs), for the daytime. Plus signs in Figure 1c show azimuths $P(\psi)$ of MS TIDs for the nighttime; the number of measurements, each of which was obtained by averaging on a 2-hour interval, totals 960. In Figure 1d, plus signs show azimuths $P(\psi)$ for the nighttime for small-scale irregularities (SSIs) for 95 days; the number of measurements, each of which was obtained by averaging on a 6-min interval, totals 1318. Solid lines in Figures 1c and 1d show the resulting azimuths $P(\psi)$, reduced to the southwestern sector. The mean values of ψ for MS TIDs and SSIs, shown by vertical dashed lines in Figures 1c and 1d, differ by about 25°. A scaled reduced curve $P(\psi) \times 0.5$ of MS TIDs (P2) for the nighttime is shown by dots in Figure 1a.

4. Diurnal-Seasonal Statistics of the Anisotropy and Dynamics of MS TIDs

Since in the literature the statistics of nighttime observations are substantially smaller compared with the daytime, it is interesting to make a general assessment of the extent to which our results differ from day to night. In order to exclude transitional processes, we combined data for the nighttime into the interval 2000-0400 LT and for combined data the daytime into 0800-1600 LT.

Figure 1 presents summary distributions. Plan solid line in Figure 1a shows azimuths $P(\psi)$ (P1), and solid line in Figure 1b shows velocities $P(v)$ of medium-scale traveling ionospheric disturbances (MS TIDs), for the daytime. Plus signs in Figure 1c show azimuths $P(\psi)$ of MS TIDs for the nighttime; the number of measurements, each of which was obtained by averaging on a 2-hour interval, totals 960. In Figure 1d, plus signs show azimuths $P(\psi)$ for the nighttime for small-scale irregularities (SSIs) for 95 days; the number of measurements, each of which was obtained by averaging on a 6-min interval, totals 1318. Solid lines in Figures 1c and 1d show the resulting azimuths $P(\psi)$, reduced to the southwestern sector. The mean values of ψ for MS TIDs and SSIs, shown by vertical dashed lines in Figures 1c and 1d, differ by about 25°. A scaled

reduced curve $P(\psi) \times 0.5$ of MS TIDs (P2) for the nighttime is shown by dots in Figure 1a.

The $P(\psi)$ distribution for the daytime (Figure 1a) has a symmetric form, with a mean value of 160° and rms of 68°. The distribution of velocities $P(v)$ Figure 1b also has a symmetric form, with a mean value of 133 m/s and rms of 62 m/s. These results agrees well with the existing more-or-less representative statistics of measurements using ionosphere-reflected HF radio waves [*Kalikhman*, 1980; *Waldock and Jones*, 1986; *Crowley et al.*, 1987] and VHF radio waves propagating through the ionosphere [*Mercier*, 1986, 1996; *Jacobson et al.*, 1995] (see also a review by *Hocke and Schlegel* [1996], and new results on a propagation characteristics of TIDs [*Ma et al.*, 1998]).

Nighttime measurements, however, provide an unexpected picture that has not been mentioned in the literature. The $P(\psi)$ for nighttime TIDs (Figure 1c, plus signs) is a symmetric two-hump distribution, with a sharply defined main maximum with the most probable values of the $\psi_{\max}$ directions 30° and 210°. In this case the direction distribution for TIDs (modulo 180°) is close to $P(\psi)$ for SSIs (Figure 1d). The only difference lies in the fact that the $P(\psi)$ for SSIs is asymmetric (the southwestward direction is more pronounced when $\psi_{\max} = 235°$).

The presence of two propagation directions simultaneously can be explained if, for some reason, the time variations of $\phi'_t(t)$ are unassociated with corresponding variations of $\phi'_x(t)$ and $\phi'_y(t)$. Such a situation arises when the propagation of the TEC wave occurs in a background of broadband random TEC fluctuations and when the TEC measurements themselves are made in a high noise level. This is equivalent to the initial method suggested by *Mercier* [1986] when only variations of $\phi'_x(t)$ and $\phi'_y(t)$ were processed. As we were unable to determine the predominant direction of propagation ψ at night, we saw little reason for comparing the velocity moduli v for MS TIDs and SSIs, and we have confined ourselves only to the comparison of the azimuthal distributions.

The difference in the distributions of $P(\psi)$ becomes clearer when ψ is determined from the modulus of 180° and when the distributions of $P(\psi)$ for both MS TIDs and SSIs are brought to one of the chosen directions (northestward or southwestward). In this case we choose the southern hemisphere, as was chosen by *Mercier* [1986, 1996], from a set of geophysical considerations and data of other independent observations. Solid lines in Figures 1c and 1d show the resulting azimuths $P(\psi)$, reduced to the southwestern sector. They are essentially symmetrical with a small spread (30°- 40°). For comparison with $P(\psi)$ for the daytime (P1), a scaled reduced

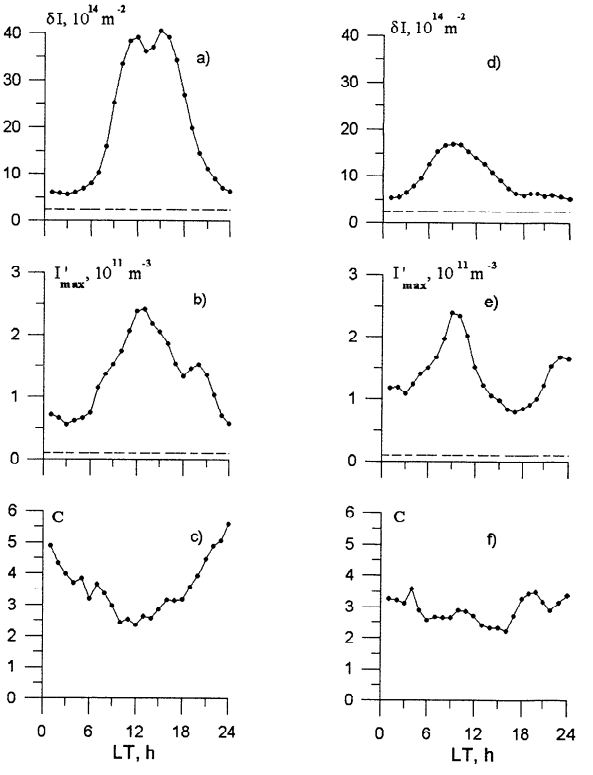

Figure 2. Diurnal dependencies of the autumn-winter (left column, 59 days) and spring-summer (right column, 61 days) average values of rms deviation of TEC variations δI (Figures 2a and 2d); rms maximum deviation of spatial derivatives of TEC $I'_{\max}$ (Figures 2b and 2e); and contrast C (Figures 2c and 2f). Horizontal dashed lines denote boundaries of the noise rms deviation of δI (Figures 2a and 2d), and $I'_{\max}$ (Figures 2b and 2e).

curve $P(\psi) \times 0.5$ of MS TIDs (P2) for the nighttime is shown by dots in Figure 1a. The mean values of ψ for MS TIDS and for SSIs, shown in Figures 1c and 1d by vertical dashed lines, differ by about 25°.

Unfortunately, there are few published nighttime measurements of TID velocities. In addition, most experimenters pointed out an instability of the TID directions at night, when it was difficult to determine a predominant propagation direction [*Waldock and Jones*, 1986; *Crowley et al.*, 1987; *Jacobson et al.*, 1995].

When analyzing the seasonal dependence, we revealed the resemblance of the characteristics for autumn-winter and spring-summer; therefore, in the subsequent discussion we discuse data for these two seasons.

Figure 2 presents diurnal dependencies of the autumn-winter (left column, 59 days) and spring-summer (right column, 61 days) average values of rms deviation of TEC variations, δI, filtered out in a selected range of periods 30–60 min (Figures 2a and 2d); of rms maximum deviation of spatial derivatives of TEC $I'_{\max}$ (Figures 2b and 2e); and in view of (2)

$$I'_{\max} = 1.61 \times \sqrt{(\phi'_x)^2 + \left(\phi'_y\right)^2} \qquad (9)$$

and of contrast C by *Mercier* [1986] (Figures 2c and 2f; see section 3). In Figure 2, horizontal dashed lines denote boundaries of the noise rms deviation of δI and $I'_{\max}$ [see *Afraimovich et al.*, 1991].

It is apparent from Figure 2 that the diurnal behavior of the relative amplitude δI of medium-scale variations in TEC for the autumn-winter (Figure 2a; the ratio of the daytime mean to nighttime value is of the order of 4-5) is more pronounced compared with the spring-summer (Figure 2d; the ratio is about 2). The diurnal dependencies presented are sufficiently consistent with the diurnal dependencies of the TEC values themselves. This is associated with the general behavior of TEC during different seasons of the year, which is pointed out in numerous publications [*Davies*, 1980; *Jacobson et al.*, 1995]. Our obtained evidence of the diurnal variability of δI is virtually identical to the data reported by *Jacobson et al.* [1995].

The spatial derivative $I'_{\max}$ during the autumn-winter (Figure 2b) shows a reasonably regular diurnal behavior, similar to the dependence of the relative amplitude δI (Figure 2a). These results correlate well with the data reported by *Mercier* [1996]. The spring-summer (Figure 2e), however, is characterized by a more complicated diurnal dependence, of which we are not yet able to give any adequate interpretation.

The diurnal dependence of the contrast C that characterizes the degree of elongation of irregularities is more pronounced for the autumn-winter (Figure 2c; the ratio of the nighttime mean to daytime value is about 2) compared with the spring-summer (Figure 2f; the ratio is close to unity). *Mercier* [1996] also points out that maximum values of the contrast reach 3.8 in winter and only 2.6 in summer, which is in quite good agreement with our data. It may be that the large values of the contrast for the nighttime (as high as 5-6) are accounted for by the fact that medium-scale, like small-scale, irregularities during the nighttime are elongated along the magnetic field (for more detail see section 5.2).

In Figure 3a (autumn-winter) and Figure 3c (spring-summer), the solid dots give the daily means of the azimuths $\psi(t)$ for waves with periods ranging from 30 to 60 min. On the basis of considerations outlined in section 4, in Figures 3a and 3c we have retained for the nighttime data only one of the alternative directions: southwestward. Interestingly, the our data agree with data of *Mercier* [1996], including a pronounced transition of the directions from southeastward to southwestward. To illustrate that our data are in good agreement with those of Mercier, in Figures 3a and 3c we marked by diamonds the data of Figure 13 of *Mercier* [1996].

Mercier [1986, 1996] points out a good agreement (with the spread of 10°) of the azimuths ψ determined by analyzing the $P(\psi)$ distribution, and in the direction of maximum contrast

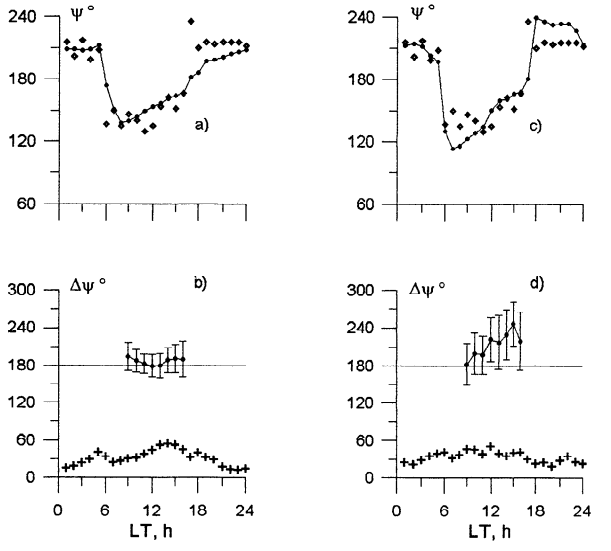

Figure 3. Diurnal dependencies of the autumn-winter (left column, 59 days) and spring-summer (right column, 61 days) average values of azimuth $\psi(t)$ (Figures 3a and 3c, dots); average values of the hourly difference $\Delta\psi = \psi - \gamma$ of propagation directions ψ of TIDs with the direction γ of the neutral wind (Figures 3b and 3d, dots); and difference of azimuths $\Delta\psi = (\psi - \psi_c)$ (Figures 3b and 3d, plus signs). Vertical bars mark off rms values. Horizontal lines in Figures 3b and 3d denote values $\Delta\psi = 180°$. Average values of $\psi(t)$ (diamonds) plotted in Figures 3a and 3c are from *Mercier* [1996].

ψ_c. We have also carried out a similar analysis of our data. Figure 3 gives mean diurnal dependencies of the difference $\Delta\psi = \psi - \psi_c$ for MS TIDs (plus signs in Figures 3b (autumn-winter) and 3d (spring-summer)). We found that almost in all seasons, the difference $\Delta\psi(t)$ gradually increases from midnight to midday, from about 15° to the maximum value of 60°, and after midday it gradually decreases. This can signify for the daytime that the propagation direction of phase inhomogeneities does not coincide with the normal to the elongation direction of the anisotropic picture of the disturbance (although this anisotropy appears only slightly during the daytime; the contrast is not over 2.5). At night, however, phase inhomogeneities are greatly elongated (the contrast is up to 5), and their apparent displacement proceeds in the direction normal to the principal axis of the dispersion ellipse.

5. Discussion and Conclusion

5.1. Verification of the "AGW Filtering by the Neutral Wind" Hypothesis

Earlier publications devoted to an experimental verification of the hypothesis of AGW filtering by the neutral wind [*Kalikhman*, 1980; *Waldock and Jones*, 1986; *Mercier*, 1986, 1996; *Crowley et al.*, 1987; *Jacobson et al.*, 1995] employed different averaged neutral wind models. For reasons of space, we will not describe our wind model used but highlight its main characteristics. It was presented partially by *Zhovty and Chernigovskaya* [1988]; a more detailed description is in preparation.

We calculated horizontal wind parameters from the equation of motion of the neutral gas with specified parameters of the thermosphere and ionosphere, with the inclusion of pressure gradients of the neutral gas, the Coriolis force, molecular viscosity, collisions with ions, and nonstationarity. Distributions of parameters of the neutral atmosphere and ionization were specified using empirical models by *Jacchia* [1977] and *Ching and Chiu* [1973], with refinements by *Anderson et al.*, [1989]. These models reasonably represent the atmospheric gas behavior at midlatitudes under undisturbed geomagnetic conditions. The geomagnetic field was calculated from the International Geomagnetic Reference Field (IGRF) model [*Langel et al.*, 1991].

At the input of a numerical model, we specified the geographical latitude of the observation site and geophysical parameters for determining the atmospheric gas distribution: day number of the year, solar activity index $F_{10.7}$, sunspot Wolf number on a given day R_z, and average (for a given day) level of magnetic disturbance Kp. Results of our calculations include height profiles of horizontal components of the neutral wind velocity vector for each hour local time of all days of the period being analyzed. For comparison with the experiment, we selected heights corresponding to the maximum of the F_2 region.

Let us now compare the measured values of ψ with those calculated using our model. Figure

3 presents diurnal dependencies of the autumn-winter (left column, 59 days) and spring-summer (right column, 61 days) average values of the hourly difference $\Delta\psi = \psi - \gamma$ of propagation directions ψ of the phase front with the direction γ of the neutral wind (solid dots in Figures 3b and 3d) during the daytime. Vertical bars denote rms values. Kp did not exceed 4.0.

The mean daytime value of $(\psi - \gamma)$ for autumn-winter was 187° with rms of about 15°. This result is in accordance with neutral wind filtering of AGW and hence MS TIDs caused by them. For the spring-summer season, however, we did not obtain evidence for the clockwise rotation for the entire day. These conclusions are readily illustrated in Figures 3c and 3d.

Of interest is the comparison of our data for the daytime with recently published results of radio interferometry with a long baseline (about 50–100 kilometers) of the signal from the geostationary satellite GOES 2 at 137-MHz frequency in New Mexico [*Jacobson et al.,* 1995]. Those measurements were carried out during a 500-day continuous run in 1993–1994. These authors found two populations (modes) of TID azimuths for daytime (southward) and nighttime (westward). New results derived by measuring AGW characteristics at the radio heliograph located at Nançay, France (47.3°N, 2.2°E), were reported by *Mercier* [1996], who analyzed measurements covering a nearly 800-hour time span of observations of radio sources of solar and non-solar origin. TID propagation directions reveal a marked spread, with the predominant direction southward. The diurnal distribution of TID azimuths clearly shows averaged southeastward directions in the daytime (mode 1) and southwestward directions at night (mode 2).

Our data on the azimuths ψ may also be represented [following *Mercier*, 1996; *Jacobson et al.,* 1995] as two populations: the daytime P1 (south-southeastward), and the nighttime P2 (southwestward), the respective distributions $P(\psi)$ for which are presented in Figure 1a. Such a representation of our data is in reasonably good agreement with the conclusions of *Mercier* [1996], which is clearly seen from the comparison of the diurnal dependencies $\psi(t)$ for our data and Mercier's in Figures 3a and 3c. We found, however (unlike *Mercier* [1996] and *Jacobson et al.* [1995]), that during the daytime the mean value of ψ increases in a clockwise direction and opposite to the calculated direction of the neutral wind.

5.2. Nighttime Irregularities

Experimental data bear witness to the elongation of SSIs along geomagnetic field lines at night and to a random character of the directivity at day [*MacDougall*, 1981; *Kumagai*, 1986]. The experiment in Hiraiso showed that in terms of a model of elliptical irregularities the direction of the principal axis of the ellipses coincides with geomagnetic field lines [*Kumagai*, 1986]. The mean value of the ratio of the principal axes ε is 6.2. The above mentioned experiments established with a high degree of reliability that the propagation directions of SSIs ψ are normal to the principal axis of the ellipse and can be calculated for a given LOS toward the radio source using appropriate models of the Earth's magnetic field. With this purpose the authors of the cited references first calculated the spatial orientation of the vector $\vec{B}$ of the magnetic field located at the selected height H above the terrestrial surface. After that, for the specified LOS toward the radio source they determined the position of the vector $\vec{P}$, which is the "radio shadow" of the vector $\vec{B}$ on the terrestrial surface; next, they calculated the direction χ of a normal to the vector $\vec{P}$. Comparison with experimental data showed that the direction χ coincides with measured values of ψ for the SSIs.

During nighttime the directions ψ of MS TIDs propagation were close (modulo 180°) to the directions of SSIs (Figures 1c and 1d). In addition, values of the contrast (up to 5–6) obtained for MS TIDs are close to the corresponding characteristics obtained for SSIs by other investigators [*MacDougall*, 1981; *Kumagai*, 1986]. The data we obtained suggest a plausible hypothesis that medium-scale irregularities at night

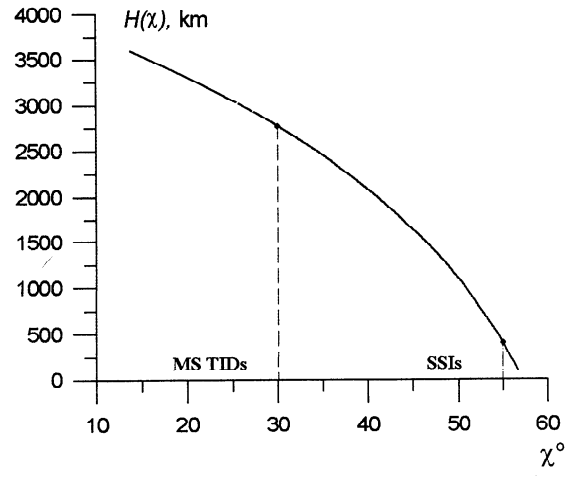

Figure 4. Dependence of altitude H from direction normal χ to the projection of the magnetic field vector onto the plane of antennas. Vertical dashed lines denote the mean values of normal ψ to the direction of stretching of MS TIDs and SSIs.

are markedly elongated along a certain direction close to the direction of elongation of SSIs. However, as is evident from Figures 1c and 1d, the most probable value of the direction for SSIs is 25° higher than that for MS TIDs, and this difference markedly exceeds the measurement error of ψ.

Using the IGRF model [*Langel et al.*, 1991], we calculated the dependence of the height $H(\chi)$ on the direction χ for the mean position of ETS 2 orbit culmination. Figure 4 presents this dependence of $H(\chi)$; vertical dashed lines denote the mean values of normal ψ to the direction of stretching of MS TIDs and SSIs (see section 4). It is evident from the dependence $H(\chi)$ that with increasing altitude, the value of the azimuth χ decreases.

Calculations showed (Figure 4) that the direction χ for height 300 kilometers altitude (the height of disposition of SSIs) is close to the mean value of ψ of SSIs (55° or 235°). This result is in agreement with known data [*MacDougall*, 1981; *Kumagai*, 1986] and gives grounds to use our obtained dependence to estimate the height H at which the irregularities elongated along the magnetic field are located and which correspond to the mean direction measured for MS TIDs. Then the mean value of ψ of MS TIDs for the nighttime (30° or 210°) can be explained if it is assumed that medium-scale phase disturbances are caused by magnetic-field-aligned irregularities located in the plasmasphere (according to our data; between 2500 and 3000 kilometers altitudes). However, such an explanation is not reconcilable with the commonly accepted concepts of the different origins of the SSIs and MS TIDs, which are most likely located in the region of maximum electron density. At the same time, this difficulty may be obviated by assuming that the medium-scale irregularities observed at night are by no means traveling wave-like processes caused by the propagation of AGWs. This issue demands further investigation.

Acknowledgments. We are grateful to V. D. Kokourov and N. N. Klimov for their great interest in this work and active participation in discussions. Thanks are also due to N. P. Minko for preparation of initial data and to V. G. Mikhalkovsky and K. S. Palamartchouk for their assistance in preparing the English version of the TEX manuscript. Great contribution was made by two referees. This work was supported by the Russian Foundation for Fundamental Research under grants 96-05-64162 and 97-02-96060. We are also indebted to the Illinois University Administration (United States) for support of this work under the Agreement on Scientific Cooperation between Illinois University and ISTP SD RAS.

References

Afraimovich, E. L., Statistical method for determining characteristics of the dynamics of the radio interference pattern, in *Proceedings of the XXVth URSI General Assembly, Lille'96, Rep. UAG-105, edited by P. J. Wilkinson*, pp. 103–108, World Data Center A for Solar-Terrestrial Physics, National Geophysical Data Center, Boulder, 1998.

Afraimovich, E. L., N. P. Minko, A. N. Shapovalov and V. N. Zvezdin, Simultaneous measurements of the polarization, angles of arrival, Doppler frequency, and amplitude of the VHF radio signal from ETS 2, *Radio Sci., 26*, 1177–1198, 1991.

Afraimovich, E. L., N. P. Minko, and S. V. Fridman, Spectral and dispersion characteristics of medium-

scale traveling ionospheric disturbances as deduced from transionospheric sounding data, *J. Atmos. Sol. Terr. Phys., 56*, 1431–1446, 1994a.

Afraimovich, E. L., G. A. Zherebtsov, V. N. Zvezdin, and S. Franke, Characteristics of small-scale ionospheric irregularities as deduced from scintillation observations of radio signals from satellites ETS 2 and Polar Bear 4 at Irkutsk, *Radio Sci., 29*, 839–855, 1994b.

Anderson, D. N., J. M. Forbes, and M. Codrescu, A fully analytic, low– and middle– latitude ionospheric model, *J. Geophys. Res., 94*, 1520–1524, 1989.

Ching, B. K., and Y. T. Chiu, A phenomenological model of global ionosphere electron density in the E-, F_1 and F_2 regions, *J. Atmos. Sol. Terr. Phys., 35*, 1615–1630, 1973.

Crowley, G., T. B. Jones, and J. R. Dudeney, Comparison of short period TIDs morphologies in Antarctica during geomagnetically quite and active intervals, *J. Atmos. Sol. Terr. Phys., 49*, 1155–1162, 1987.

Davies, K., Recent progress in satellite radio beacon studies with particular emphasis on the ATS-6 radio beacon experiment, *Space Sci. Rev., 25*, 357–430, 1980.

Georges, T. M., HF Doppler studies of traveling ionospheric disturbances, *J. Atmos. Sol. Terr. Phys., 30*, 735–746, 1968.

Georges, T. M., and W. H. Hooke, Wave-induced fluctuations in ionospheric electron content: A model indicating some observational biases, *J. Geophys. Res., 75*, 6295–6308, 1970.

Hines, C. O., and C. A. Reddy, On the propagation of atmospheric gravity waves through regions of wind shear, *J. Geophys. Res., 72*, 1015-1034, 1967.

Hocke, K., and K. Schlegel, A review of atmospheric gravity waves and traveling ionospheric disturbances: 1982-1995, *Ann. Geophys., 14*, 917–940, 1996.

Jacchia, L. G., Thermospheric temperature, density and composition: New models, *Spec. Rep. 375*, Smithson. Inst. Astrophys. Obs., Cambridge, Mass., 1977.

Jacobson, A. R., R. C. Carlos, R. S. Massey, and G. Wu, Observations of traveling ionospheric disturbances with a satellite-beacon radio interferometer: Seasonal and local time behavior, *J. Geophys. Res., 100*, 1653–1665, 1995.

Jacobson, A. R., G. Hoogeveen, R. C. Carlos, G. Wu, B. G. Fejer, and M. C. Kelley, Observations of inner plasmasphere irregularities with a satellite-beacon radio-interferometer array, *J. Geophys. Res., 101*, 19, 665-19,682, 1996.

Kalikhman, A. D., Medium-scale traveling ionospheric disturbances and thermospheric winds in the F-region, *J. Atmos. Sol. Terr. Phys., 42*, 697–703, 1980.

Kumagai, H., Behavior of mid-latitude F-region irregularities deduced from spaced-receiver VHF scintillation measurements, *J. Atmos. Sol. Terr. Phys., 48*, 221–230, 1986.

Langel, R. A., et al., International Geomagnetic Reference Field (IGRF) revision, *J. Geomagn. Geoelectr., 43*, 1007–1012, 1991.

Ma, S. Y, K. Schlegel, and J. S. Xu, Case studies of the propagation characteristics of auroral TIDs with EISCAT CP2 data using maximum entropy cross-spectral analysis, *Ann. Geophys., 16*, 161–167, 1998.

MacDougall, J. W., Distributions of the irregularities which produce ionospheric scintillations, *J. Atmos. Sol. Terr. Phys., 43*, 317–325, 1981.

Mercier, C., Observations of atmospheric gravity waves by radio-interferometry, *J. Atmos. Sol. Terr. Phys., 48*, 605–624, 1986.

Mercier, C., Some characteristics of atmospheric gravity waves observed by radio-interferometry, *Ann. Geophys., 14*, 42–58, 1996.

Waldock, J. A., and T. B. Jones, HF Doppler observations of medium-scale traveling ionospheric disturbances at mid-latitudes, *J. Atmos. Sol. Terr. Phys., 48*, 245–260, 1986.

Zhovty, E. I., and M. A. Chernigovskaya, The model of large-scale movements and electric fields in the middle- and low-latitude ionosphere (in Russian), in *Researching of the Dynamics Processes in the Upper Atmosphere*, pp. 267–271, Gidrometeoizdat, Moscow, Russia, 1988.

E. L. Afraimovich, O. N. Boitman, A. D. Kalikhman, and T. G. Pirog, Institute of Solar-Terrestrial Physics, 664033 Irkutsk, p. o. box 4026, Russia. (e-mail: afra@iszf.irk.ru)

(Received May 18, 1998;
revised September 14, 1998;
accepted September 15, 1998.)